

## Crystal Structure Elucidation

The Long-Periodic Loop-Branched Chain Structure of the Oxonitridophosphate  $\text{La}_{21}\text{P}_{40}\text{O}_{46}\text{N}_{57}$ , Elucidated by a Combination of TEM and Microfocused Synchrotron RadiationMarkus Nentwig,<sup>[a]</sup> Simon D. Kloß,<sup>[b]</sup> Lukas Neudert,<sup>[b]</sup> Lucien Eisenburger,<sup>[b]</sup> Wolfgang Schnick,<sup>[b]</sup> and Oliver Oeckler<sup>\*[a]</sup>

**Abstract:** The lanthanum oxonitridophosphate  $\text{La}_{21}\text{P}_{40}\text{O}_{46}\text{N}_{57}$  was synthesized by high-pressure metathesis from partially hydrolysed  $\text{LiPN}_2$  and  $\text{LaCl}_3$  at 750–950 °C and 7–9 GPa. The combination of transmission electron microscopy (TEM) and diffraction using microfocused synchrotron radiation revealed a monoclinic crystal structure (space group  $P2_1/n$ ,  $a = 14.042(4)$ ,  $b = 7.084(3)$ ,  $c = 41.404(10)$  Å,  $\beta = 97.73(3)^\circ$  and  $Z = 2$ ), which is characterized by loop-branched 21 member single chains of  $\text{P}(\text{O},\text{N})_4$  tetrahedra that extend along [201]. These chains are related to the loop-branched *dreier* single

chains with *dreier*-ring loops in stillwellite ( $\text{CeBSiO}_5$ ). In  $\text{La}_{21}\text{P}_{40}\text{O}_{46}\text{N}_{57}$ , these chains are characterized by a complex long-periodic conformation and exhibit disorder that involves La/N and P split positions. This is an extraordinarily long periodicity with respect to branched single chains of tetrahedra.  $\text{La}_{21}\text{P}_{40}\text{O}_{46}\text{N}_{57}$  constitutes the first rare-earth oxonitridophosphate exhibiting a chain structure. Single-crystal data are consistent with electron and powder X-ray diffraction.

## Introduction

Among solid-state compounds with crystal structures built up from tetrahedral entities, silicates feature an extraordinarily diverse structural chemistry. Extensive combinations of metal cations and a plethora of chemical compositions lead to a large variety of silicate substructures.<sup>[1]</sup> Almost all silicates contain  $\text{SiO}_4$  tetrahedra as primary building units (PBUs) derived from hypothetical silicic acid and its isopolyacids, resulting in polyanions extending in 0, 1, 2 or 3 dimensions. Chains of vertex-sharing  $\text{SiO}_4$  tetrahedra, for instance, represent a large structural family of silicate minerals. The longest unbranched silicate chains reported so far comprise *neuner* (9er, ferrosilite III),<sup>[2]</sup> *zwölf* (12er, alamosite),<sup>[3]</sup> and *vierundzwanziger* (24er,  $\text{Na}_{24}\text{Y}_8[\text{Si}_{24}\text{O}_{72}]$ , synthetic)<sup>[4]</sup> single chains.<sup>[5]</sup> Other values of the periodicity are known from structurally related phosphates, for

example, *zehner* single chains in the polyphosphate  $\text{K}_2\text{Ba}_4[\text{P}_{10}\text{O}_{30}]$ .<sup>[6]</sup> Branched single chains with tetrahedra that are not part of the main chain, for example, open-branched *vierer* (4er) single chains in aenigmatite,<sup>[7]</sup> loop-branched *achter* (8er) chains in pellyite,<sup>[8]</sup> *zehner* (10er) chains in nordite,<sup>[9]</sup> or *vierzehner* (14er) in liebauite,<sup>[10]</sup> complement the group of inosilicates.

The combination of different kinds of tetrahedra, for example,  $\text{BO}_4$  and  $\text{SiO}_4$ , extends the structural diversity and leads to further single-chain structures like loop-branched *dreier* chains with *dreier*-ring loops as described for the mineral stillwellite  $\text{CeBSiO}_5$  (space group  $P3_1$ ,  $a = 6.85$ ,  $c = 6.70$  Å).<sup>[11]</sup> Its rather simple crystal structure is characterized by  $\text{Ce}_3[\text{B}_3\text{Si}_3\text{O}_{15}]$  units consisting of a helical *dreier* single chain of  $\text{BO}_4$  tetrahedra with three loop-branches that involve additional  $\text{SiO}_4$  tetrahedra. This structure type has also been reported for borogermanates  $M[\text{BGeO}_5]$  with  $M = \text{La}$ ,  $\text{Pr}$ <sup>[12]</sup> and borophosphates  $M[\text{BPO}_5]$  with  $M = \text{Ca}$ ,  $\text{Sr}$ ,  $\text{Ba}$ ,  $\text{Pb}$ .<sup>[13]</sup> Such anionic substructures have not yet been obtained with only one kind of tetrahedral PBU. However, formally replacing B in such borophosphates by P leads to  $\text{P}_2\text{O}_5$  and the formal exchange of O by N leads to a charged polyanion.

Nitridophosphates are expected to have an extended structural diversity compared to oxophosphates, owing to a larger range for the degree of condensation and the possibility of triply bridging N atoms. With mixed O/N atom positions in oxonitridophosphates, the structural diversity may be further increased, and the few known examples feature an intriguing structural chemistry with unique building blocks.  $\text{LiPr}_2\text{P}_4\text{N}_7\text{O}_3$ , for example, is the first nitridophosphate with single layers of

[a] M. Nentwig, Prof. Dr. O. Oeckler  
Institute of Mineralogy, Crystallography and Materials Science  
Leipzig University, Scharnhorststraße 20, 04275 Leipzig (Germany)  
E-mail: oliver.oeckler@gmx.de

[b] Dr. S. D. Kloß, Dr. L. Neudert, L. Eisenburger, Prof. Dr. W. Schnick  
Department of Chemistry, University of Munich (LMU)  
Butenandstraße 5–13 (D), 81377 Munich (Germany)

Supporting information and the ORCID identification number(s) for the author(s) of this article can be found under:  
<https://doi.org/10.1002/chem.201902873>.

© 2019 The Authors. Published by Wiley-VCH Verlag GmbH & Co. KGaA. This is an open access article under the terms of Creative Commons Attribution NonCommercial-NoDerivs License, which permits use and distribution in any medium, provided the original work is properly cited, the use is non-commercial and no modifications or adaptations are made.

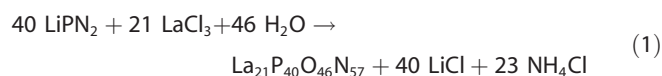
tetrahedra,<sup>[14]</sup> while  $\text{CaMg}_2\text{P}_6\text{O}_3\text{N}_{10}$ <sup>[15]</sup> and  $\text{Hf}_{9-x}\text{P}_{24}\text{N}_{52-4x}\text{O}_{4x}$  ( $x \approx 1.84$ )<sup>[16]</sup> crystallize in the  $\text{Ti}_5\text{B}_{12}\text{O}_{26}$  type with interpenetrating adamantanoid (diamond-like) tetrahedra frameworks. Although multinary systems like oxonitridophosphates, in principle, offer a greater variety with respect to composition and structure,<sup>[17]</sup> but are often underdeveloped when compared to the parent classes of compounds, for example, oxophosphates and nitridophosphates. For example, only two chain-type oxonitridophosphates have been described in literature, namely  $\text{Li}_2\text{PO}_2\text{N}$ <sup>[18]</sup> and  $\text{Ba}_6\text{P}_{12}\text{N}_{17}\text{O}_9\text{Br}_3$ .<sup>[19]</sup> Examples with rare earth metals have been unknown so far. However, high-pressure metathesis has been shown to be a successful approach to rare-earth nitridophosphates.<sup>[20]</sup> The presence of hydrolysis products during high-pressure synthesis has, for example, led to the complex intergrown structure of  $\text{Ce}_{4-0.5x}\text{Li}_3\text{P}_{18}\text{N}_{35-1.5x}\text{O}_{1.5x}$  ( $x \approx 0.72$ ).<sup>[21]</sup>

In this contribution we report on  $\text{La}_{21}\text{P}_{40}\text{O}_{46}\text{N}_{57}$ , the first rare-earth representative of chain-type oxonitridophosphates. Its complicated loop-branched *21er* single chains involve an unusually large lattice parameter. In combination with the fact that the title compound was obtained as a microcrystalline reaction product including a side phase, this impeded structure analysis both by conventional single-crystal diffraction and by powder diffraction methods. A combination of TEM and diffraction of microfocused synchrotron radiation was required to obtain precise structural data.

## Results and Discussion

### Synthesis and sample characterization

$\text{La}_{21}\text{P}_{40}\text{O}_{46}\text{N}_{57}$  was prepared from  $\text{LiPN}_2$  (see Experimental Section)<sup>[22]</sup> and  $\text{LaCl}_3$  by high-pressure metathesis at either 7 GPa and 750 °C or 9 GPa and 950 °C using the multianvil technique. This reaction, followed by washing with diluted HCl and water, afforded a colourless heterogenous mixture of  $\text{La}_{21}\text{P}_{40}\text{O}_{46}\text{N}_{57}$  and the starting material  $\text{LiPN}_2$ . The oxygen in the product originates from hydrolysis of either  $\text{LaCl}_3$  or the used BN crucible and is accounted for in the reaction equation by  $\text{H}_2\text{O}$  [Eq. (1)]:



Depending on the reaction conditions, the products contain up to more than 85% (higher pressure/ temperature) of  $\text{La}_{21}\text{P}_{40}\text{O}_{46}\text{N}_{57}$  according to Rietveld refinements based on powder X-ray diffraction (PXRD) data (Figure S1 and S2, S denotes figures and tables in the in the Supporting Information) using the structure model derived from single-crystal data (see below). The elemental composition was determined by energy dispersive X-ray spectroscopy (EDX) in combination with TEM. Data of several crystallites confirm the atomic ratio La/P of 21:40 (Table S1) obtained in the structure refinement. The infrared spectra show the characteristic fingerprint of oxonitridophosphates at  $< 1500 \text{ cm}^{-1}$  (Figure S3),<sup>[23]</sup> which corresponds to phosphate framework vibrations. The very weak signal at ca.

$3250 \text{ cm}^{-1}$  corresponds to N–H or O–H modes that might be due to a small amount of surface hydrolysis. Therefore, hydrogen was not taken into account in the crystal structure analysis.

### Structure determination

The crystal structure was solved and refined from single-crystal data obtained from a microcrystal (Figure S4). The crystal was selected with the aid of TEM imaging and characterized by EDX and electron diffraction, which indicated an unknown crystal structure. The position of the crystal on the TEM grid was identified at the synchrotron by means of an optical telescope and fluorescence scans.<sup>[24]</sup> Diffraction data were then collected using a microfocused beam. Crystallographic data including the atomic coordinates and displacement parameters are listed in Table 1, and Tables S2 and S3. The unit-cell parameters were taken from powder X-ray diffraction data (Figure S1). The initial structure solution revealed eleven atom positions occupied by La. Unusually large atomic displacement parameters were initially observed for the La11 atoms, which turned out to share their positions with N atoms of vertex-sharing  $\text{PN}_4$  tetrahedra around the P12 and P17 atoms (Figure S5). An inversion centre (in the middle of the unit-cell edges) further relates La11 to a symmetry-equivalent position at a distance of approximately 2.4 Å, which is too short to correspond to a La–La distance. The site occupancy factor (s.o.f.) of La11, however, refines to ca. 56%, which equals an integrated electron density of 32 electrons. This matches the average number of electrons of La (57 electrons) and N (7 electrons). A small amount of oxygen on this position was taken into account for the sake of charge neutrality as described below. The situation can thus be interpreted assuming disorder of  $\text{N52/O52}$  and La11 at the same position in combination with presence or absence of  $\text{P(O,N)}_4$  tetrahedra of the central atoms P12 and P17. As La11 is not present at both positions simulta-

**Table 1.** Crystallographic data of the single-crystal structure refinement of  $\text{La}_{21}\text{P}_{40}\text{O}_{46}\text{N}_{57}$ .

Sum formula	$\text{La}_{21}\text{P}_{40}\text{O}_{46}\text{N}_{57}$
formula mass / $\text{g mol}^{-1}$	5690.3
space group	$P2_1/n$ (no. 14)
cell parameters / Å, °	$a = 14.042(4)$ , $b = 7.084(3)$ $c = 41.404(10)$ , $\beta = 97.73(3)$
cell volume / Å <sup>3</sup>	4081(2)
X-ray density / $\text{g cm}^{-3}$	4.63
formula units per unit cell	2
$F(000)$	5128
temperature / K	295
radiation	synchrotron (ESRF, ID11), $\lambda = 0.30900 \text{ Å}$
$\theta$ range / °	1.49–13.75
$\mu$ / $\text{mm}^{-1}$	6.413
reflections meas./indep.	47 670 / 14 508
$R_{\text{int}}$ ; $R_{\sigma}$	0.0972; 0.0216
parameters	514
$R1$ [ $I > 2\sigma(I)$ ] / $R1$ (all)	0.0669 / 0.1240
$wR$ [ $I > 2\sigma(I)$ ] / $wR$ (all)	0.0769 / 0.0888
$\text{Goof}$	1.90
$\Delta\rho$ (min./max., $\text{e Å}^{-3}$ )	–2.14 / 3.98

neously, there is no unrealistically short La11-La11 distance in the actual structure. A corresponding refinement leads to s.o.f.'s of 0.513(4) for La11 and 0.487(4) for N52/O52, P12 and P17. As the deviation from equal probabilities was not significant, the s.o.f.'s were set to 0.5 and treated as a symmetry-enforced split position. A second split position is located around other inversion centres at the corners and the centre of the unit cell (Figure S6). This position involves disordered P(N,O)<sub>4</sub> tetrahedra with two P and six N/O atom positions, which leads to four possible interconnection patterns of the tetrahedra. Again, the refinement of s.o.f.'s shows no deviation from equal probabilities (P6, N49, O42, O35: s.o.f.=0.501(10) and P22, O49, N42, O35': s.o.f.=0.499(10)), the corresponding s.o.f.'s were set to 0.5.

In order to confirm that this is true disorder and not a symmetry-related artefact, refinements in the non-centrosymmetric space group *Pn* were carried out for comparison. Although the much larger number of refined parameters slightly decreases the *R* values (*R*(obs)=0.0640, *wR*(obs)=0.0758), symmetry reduction and taking into account inversion twinning does not remove the disorder at the mentioned split positions. In *Pn*, these are not, symmetry-related. Yet, *F*<sub>obs</sub> Fourier maps still show equal electron density at both positions and electron densities at position where an "idealized" structure would have no atoms remain clearly visible in difference Fourier maps (Figure 1). Thus, the disorder cannot be resolved using lower symmetry than *P2*<sub>1</sub>/*n*.

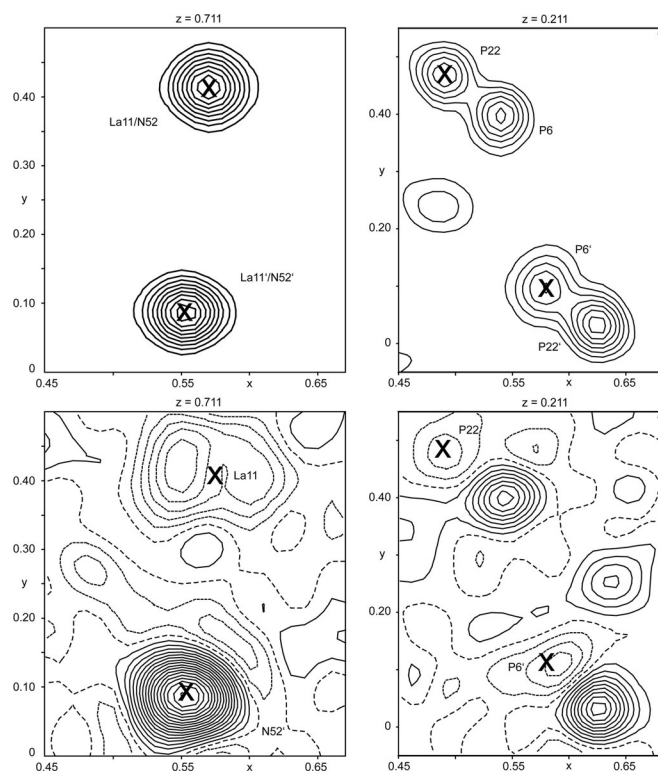


**Figure 1.** *F*<sub>obs</sub> Fourier (top, contour interval 7 e<sup>Å</sup><sup>-3</sup>) and difference Fourier (bottom, contour interval 0.5 e<sup>Å</sup><sup>-3</sup>) maps around the two split positions of the crystal structure, based on a model refined in space group *Pn* (taking into account inversion twinning); crosses represent the "idealized" positions of La11/N52 (left) and P6/P22 (right).

Since O and N atoms can hardly be distinguished by X-ray scattering, terminal atoms were initially assumed to be O and bridging atoms were assumed to be N in line with Pauling's rules, which results in the sum formula [La<sub>21</sub>P<sub>40</sub>O<sub>42</sub>N<sub>61</sub>]<sup>4-</sup>. In order to achieve a charge neutral sum formula La<sub>21</sub>P<sub>40</sub>O<sub>46</sub>N<sub>57</sub>, all of the N atom positions, except N42 and N49, which are involved in the P split position, were partially occupied with 6.78% [= 4/59 = (negative charges)/(number of N atoms except N42 and N49)] of O atoms. This mixed site occupation is not shown in the structure images for the sake of clarity. The small sample volume in high-pressure syntheses and the facts that the product is not phase-pure and shows pronounced reflection overlap in powder patterns due to the large monoclinic unit cell impeded the distinction of O and N by neutron diffraction. The comparison of calculated diffraction patterns (based on the structure model from single-crystal data) with corresponding reciprocal lattice sections (*0kl*, *h0l* and *hk0*) confirms the metrics and the structure model (Figure 2, larger reciprocal lattice sections are displayed in Figure S7). The large number of weak reflections is a characteristic feature of this wave-like structure. This results in clusters of reflections that, at first glance, might suggest the a description as a commensurately modulated structure with a (3+1)D superspace approach. However, a closer inspection of the reciprocal lattice, for example, its sections *0kl* and *h1l* (Figure S8) shows that the

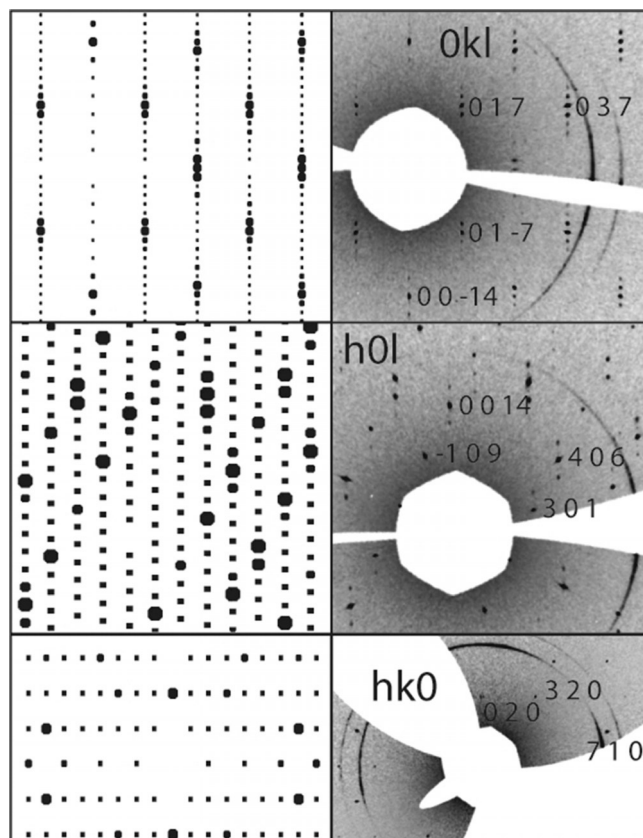


**Figure 2.** Simulated X-ray diffraction pattern based on the single-crystal data (left) and reconstructed reciprocal lattice sections (right,  $\lambda = 0.29470$  Å) with selected indexed reflections. The diffraction rings originate from the polycrystalline Cu of the TEM grid, which was used to support the crystallite.

reflections corresponding to a hypothetical basic cell are sometimes weaker and sometimes stronger than the “satellites”. In addition, almost 50% of the reflections corresponding to the 3D lattice are observed with intensities larger than three standard deviations. In conclusion, a commensurately modulated description would have a basic structure with partial occupancy of all atoms and would require many parameters to derive the correct structure by applying occupational modulation waves. Together with the complex disorder in this compound, this would certainly not be a benefit for the structure refinement.

In TEM investigations, crystallites of the title compound can easily be recognized by their characteristic diffraction patterns (Figure S9). Figure S10 shows a comparison of experimental and simulated selected area electron diffraction (SAED) patterns of the crystal used for synchrotron data collection; the corresponding tilt angles are displayed in Figure S11.

### Structure description

The crystal structure of  $\text{La}_{21}\text{P}_{40}\text{O}_{46}\text{N}_{57}$  (Figure 3) is characterized by chains of corner-sharing  $\text{P}(\text{N},\text{O})_4$  tetrahedra that extend

along [201]. According to Liebau's nomenclature,<sup>[1]</sup> this results in a hybrid-branched *21er* single chain with the formula  $\text{La}_{21}\{\text{hB}, 1^1_{\infty}\} [\text{P}_{21}(\text{N},\text{O})_{63}(\text{P}(\text{N},\text{O})_{17}(\text{P}(\text{N},\text{O})_{32})_2]$ , derived from the formula for loop-branched single chain silicates  $\{\text{B}, 1^1_{\infty}\} [\text{Si}_p\text{O}_{2.5p}]^{3p}$  (*B*: loop-branched, *P*: periodicity, *p*: number of all tetrahedral centres). The first part in the formula of  $\text{La}_{21}\text{P}_{40}\text{O}_{46}\text{N}_{57}$  corresponds to the single chain  $(\text{P}_{21}(\text{N},\text{O})_{63})$ , followed by the loop-branches  $(\text{P}_{17}(\text{N},\text{O})_{34})$  and the open branches  $(\text{P}_2(\text{N},\text{O})_6)$  (located at the disordered positions). Since the interconnection of these units is disordered, the chains are either interconnected to each other along [201] through corner- or edge-sharing  $\text{P}(\text{N},\text{O})_4$  tetrahedra or not connected. These disordered tetrahedra (marked in green in Figure 3) are located near inversion centres (centre, corner and centre of the edges of the unit cell, Figure 3 a), which results in different possible modes of interconnection of the chains. There are two possible variants for the split position in the middle of the chain (Figure S5) and four for the other split position (Figure S6) located at the end of the chain, as displayed in Figure 3 b. This results in eight possible combinations of the two disordered positions. According to Pauling's rules, hypothetical combinations with vertex-sharing tetrahedra (Figure S12) are more likely than the

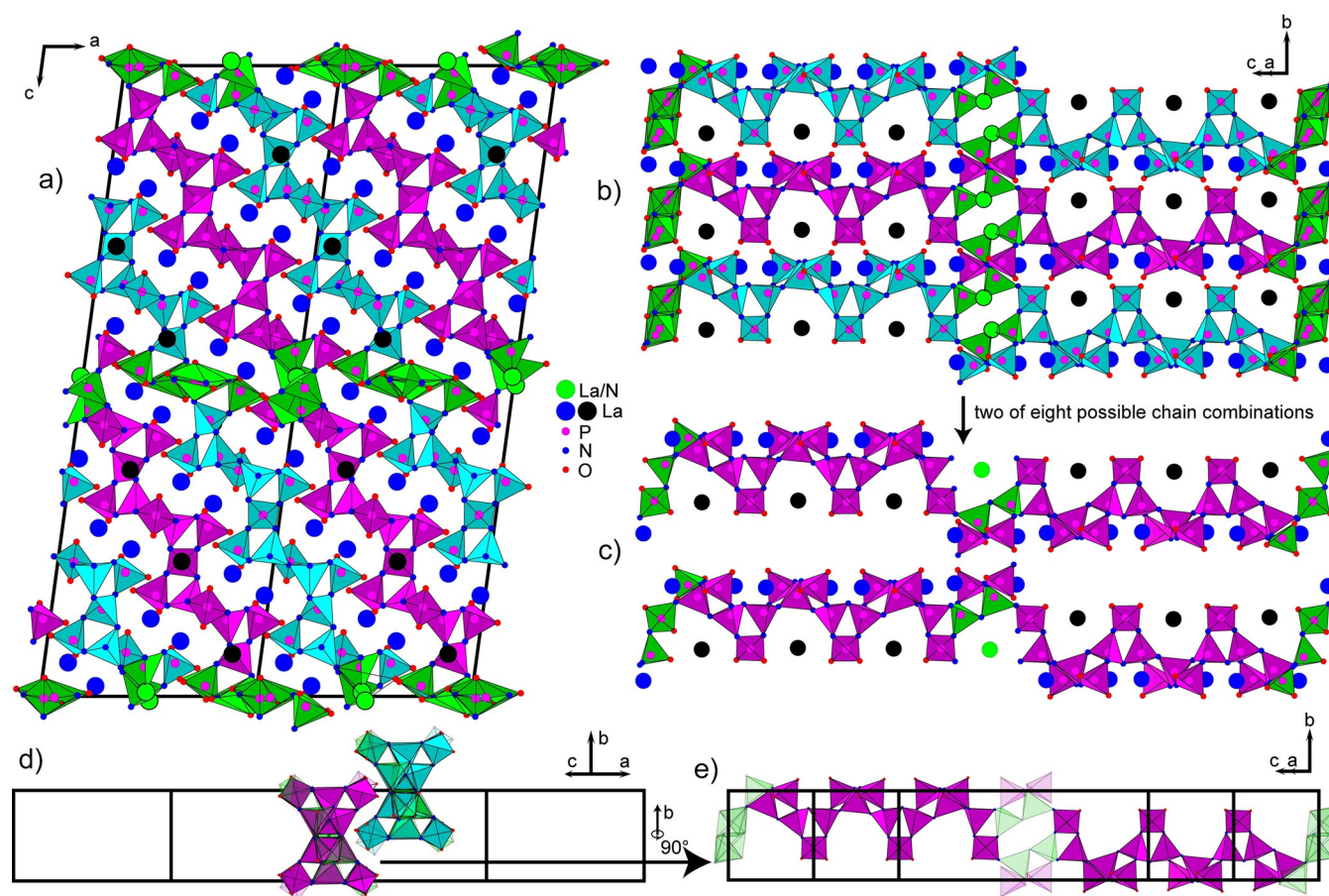


**Figure 3.** Crystal structure of  $\text{La}_{21}\text{P}_{40}\text{O}_{46}\text{N}_{57}$  viewed along [010] (a) and perpendicular to [010] (b).  $\text{P}(\text{N},\text{O})_4$  tetrahedra and La atoms involved in split positions are displayed in green; unaffected tetrahedra are magenta or blue. La atoms are distinguished by different colours (black/green and blue) according to their different packing in the structure as seen in (a). Further images show two of eight possible structures of the chain (combination 1 and 4 from Figure S12) (c) and representative parts of the crystal structure of  $\text{La}_{21}\text{P}_{40}\text{O}_{46}\text{N}_{57}$  along [201] (d) and rotated by  $90^\circ$  (e). A part of the chain, which is unaffected by the disorder, consists of a loop-branched *achter* single chain of tetrahedra  $[\text{P}_{16}(\text{N},\text{O})_{48}]$  and is emphasized in magenta; tetrahedra involved in split positions are depicted in a transparent manner.

combinations with edge-sharing or not connected tetrahedra (Figure S13). However, the P-N/O bond lengths of the tetrahedra involved in this split position do not indicate a preferred combination (Table S4). All tetrahedra in the structure exhibit interatomic distances between partially disordered P and N/O positions in the range of 1.3–1.8 Å, corresponding to values reported for other oxonitridophosphates mentioned in the Introduction. Note however, that in the case of disordered P atoms, average positions for O/N were used, which explain some seemingly too small or too large values. The La atoms are coordinated by nine N/O atoms forming irregular polyhedra with La–N/O bond lengths in the range of 2.4–3.0 Å, which are comparable to those in  $\text{La}_2\text{P}_3\text{N}_7$  and  $\text{LaPO}_4$ .<sup>[25,26]</sup> As an example for the chain structure, two of the eight possible combinations of the two split positions are additionally shown in Figure 3c. A view along the chain displays the packing of the structure (Figure 3d; a larger part of the structure with views along different directions is shown in Figure S14). The cut-outs of the chain that are unaffected by the disorder, may be described as loop-branched *achter* single chains [ ${}^{\text{P}}\text{P}_{16}(\text{N},\text{O})_{40}$ ] (Figure 3e).

A related chain structure has been described for the mineral stillwellite ( $\text{CeBSiO}_5$ ),<sup>[11]</sup> which is built up exclusively from loop-branched *dreier* single chains along [001]. It crystallizes in the space group  $P3_1$  and exhibits *dreier* single chain of  $\text{BO}_4$  tetrahedra with loop-branches of  $\text{SiO}_4$  tetrahedra, corresponding to the formula  $\text{Ce}_3\{B, 1^{\infty}\}[\text{B}_3\text{O}_9(\text{SiO}_2)_3]$  (Figure S15). In contrast, the chains in  $\text{La}_{21}\text{P}_{40}\text{O}_{46}\text{N}_{57}$  are built up exclusively from  $\text{P}(\text{O},\text{N})_4$  tetrahedra, which form a corrugated arrangement, resulting in the long-periodic chain structure (Figure S16).

## Conclusions

A new lanthanum oxonitridophosphate  $\text{La}_{21}\text{P}_{40}\text{O}_{46}\text{N}_{57}$  with a long-periodic chain structure was obtained by high-pressure synthesis in conjunction with partial hydrolysis. This type of reaction might lead to numerous mixed anion compounds if the oxygen-containing species is added deliberately in an inert reaction environment. To the best of our knowledge, this is the first chain-like rare-earth oxonitridophosphate and exhibits the longest periodicity of branched single chains of tetrahedra observed so far. Its structure is characterized by loop-branched *21er* single chains of  $\text{P}(\text{O},\text{N})_4$  tetrahedra, which is the longest periodicity for a branched tetrahedral chain observed so far. However, there is certain disorder, which may involve occasional interruptions in the chains. This unusually complicated chain structure gives further precedence to the structural diversity one can expect in multinary phosphate systems. As it is the case in many high-pressure syntheses, the reaction product is microcrystalline and not homogeneous. Thus, the crystal structure determination demonstrates the potential of combining TEM investigations with diffraction data obtained by microfocused synchrotron radiation. Such refinement results are significantly more precise than most parameters from electron crystallography or Rietveld refinements on powder data. This new approach of single-particle diffraction analysis could give access to unexplored high-pressure oxonitridophosphates exhibiting new tetrahedral structures.

## Experimental Section

### LiPN<sub>2</sub>

For the preparation of lithium nitridophosphate  $\text{LiPN}_2$ ,  $\text{P}_3\text{N}_5$  was first obtained by ammonolysis of tetraphosphorus decasulfide ( $\text{P}_4\text{S}_{10}$ ) as described by Grüneberg and Stock.<sup>[27]</sup>  $\text{LiPN}_2$  was then prepared through reaction of  $\text{P}_3\text{N}_5$  and a 1.2-fold excess of  $\text{Li}_3\text{N}$  at 850 °C for 96 h. The starting materials were thoroughly mixed and ground under inert conditions in a glovebox (<1 ppm  $\text{H}_2\text{O}$ , <1 ppm  $\text{O}_2$ ), then transferred into a Ta ampule which was subsequently sealed in a dried fused silica ampoule under inert gas atmosphere. The brownish product was washed with diluted hydrochloric acid followed by water. The phase composition of the compound was verified by PXRD, EDX and IR spectroscopy.

### La<sub>21</sub>P<sub>40</sub>O<sub>46</sub>N<sub>57</sub>

The title compound was prepared by high-pressure high-temperature synthesis using  $\text{LaCl}_3$  (Alfa Aesar, 99.99%). The reaction conditions of either 7 GPa and 750 °C or 9 GPa and 950 °C were achieved with a hydraulic 1000 t press (Voggenreiter, Mainleus, Germany) applying the multianvil technique. An h-BN crucible of the 18/11-assembly size (cavity diameter = 1.6 mm, cavity depth = 2.3 mm) was loaded with the starting materials in a glovebox (<1 ppm  $\text{H}_2\text{O}$ , <1 ppm  $\text{O}_2$ ). The crucible was placed inside an 18/11-assembly sized octahedron consisting of  $\text{Cr}_2\text{O}_3$ -substituted (6%) MgO (Ceramic Substrates & Components, Isle of Wight, U.K.). Eight tungsten carbide (with 7% Co) cubes (Hawedia, Marklkofen, Germany) with truncated edges (edge length = 11 mm) were used as anvils. The sample was first pressurized then heated with 7.75  $\text{Kmin}^{-1}$  and 300 min dwell time at 750 or 950 °C. Additional information regarding high-pressure/high-temperature synthesis can be found in literature.<sup>[28]</sup> The product was obtained as a colourless powder, which was washed with  $\text{H}_2\text{O}$  to remove residual  $\text{LiCl}$  and  $\text{NH}_4\text{Cl}$ .

### Powder X-ray diffraction

PXRD of samples in glass capillaries (0.2 mm diameter) was carried out on a STOE STADI P diffractometer with modified Debye–Scherrer geometry using  $\text{MoK}_{\alpha 1}$  and  $\text{CuK}_{\alpha 1}$  radiation (Stoe & Cie., Darmstadt, Germany, Ge(220) and Ge(111) monochromator; Mythen1K detector, DECTRIS Ltd., Switzerland). For Rietveld refinements, TOPAS Academic V5.0<sup>[29]</sup> was used, applying the fundamental parameters approach. Preferred orientation was described by spherical harmonics of fourth order.

### Fourier-transform infrared spectroscopy

FTIR spectra of  $\text{La}_{21}\text{P}_{40}\text{O}_{46}\text{N}_{57}$  were recorded under ambient conditions on a Spectrum BX II spectrometer with DuraSampler ATR device (Perkin Elmer).

### Transmission electron microscopy

Small amounts of  $\text{La}_{21}\text{P}_{40}\text{O}_{46}\text{N}_{57}$  were ground in absolute ethanol and drop-cast on copper finder grids covered with carbon film (Plano GmbH, Germany). The grids were mounted on a double-tilt holder and transferred into a Cs DCOR probe-corrected Titan Themis 300 TEM (FEI, USA) operated at 300 kV, equipped with X-FEG, post-column filter (Enfinium ER-799) and a windowless, 4-quadrant Super-X EDX detector. SAED and EDX were used to identify suitable crystals for structure determination. TEM images were recorded using a 4k × 4k FEI Ceta CMOS camera. Maps of the grids enable subsequent positioning of the selected crystals in the syn-

chrotron beam. TEM data were evaluated with Digital Micrograph (SAED patterns),<sup>[30]</sup> ProcessDiffraction7,<sup>[31]</sup> JEMS (SAED simulations),<sup>[32,33]</sup> and ES Vision (EDX).<sup>[34]</sup>

### Single-crystal X-ray diffraction

Single-crystal data of a crystallite on a copper finder grid were collected at beamline ID11 of the European Synchrotron Radiation Facility (ESRF, Grenoble) using microfocused synchrotron radiation. The crystal was centred in a beam of  $\approx 2 \mu\text{m}$  diameter with the help of fluorescence scans using the  $\text{La}_{\text{K}\alpha}$  emission lines. Diffraction data were recorded with a Frelon4k CCD detector.<sup>[35]</sup> Integration and semiempirical absorption correction were performed with CrysAlisPro.<sup>[36]</sup> Two datasets were scaled to one reflection file using XPREP.<sup>[37]</sup> A correction for incomplete absorption of high-energy radiation in the phosphor of the CCD detector was applied.<sup>[38]</sup> The structure was solved with SHELX,<sup>[39]</sup> and the refinement as well as the calculation of Fourier sections and simulation of diffraction patterns was performed with JANA.<sup>[40]</sup> Crystal structures were visualized with Diamond.<sup>[41]</sup> CCDC 1903490 contain the supplementary crystallographic data for this paper. These data are provided free of charge by The Cambridge Crystallographic Data Centre.

### Acknowledgements

The authors thank Dr. Jonathan Wright and Dr. Vadim Dyadkin (ESRF, Grenoble), as well as Dr. Christopher Benndorf, Daniel Günther, Dr. Frank Heinke, Peter Schultz, Stefan Schwarzmüller and Tobias Stollenwerk (Leipzig University) for their help with synchrotron measurements and the ESRF for granting beamtime (projects CH-5142 and CH-4612). Financial support provided by the Deutsche Forschungsgemeinschaft (projects OE530/6-1 and SCHN377/18-1) and a PhD fellowship from the Fonds der Chemischen Industrie (FCI) for S.D.K. are gratefully acknowledged.

### Conflict of interest

The authors declare no conflict of interest.

**Keywords:** chain structures · high-pressure/high-temperature chemistry · metathesis · microcrystals · rare-earth oxonitridophosphate

- [1] F. Liebau, *Structural Chemistry of Silicates*, Springer, Heidelberg, 1985.
- [2] H. P. Weber, *Acta Crystallogr. Sect. C* **1983**, 39, 1–3.
- [3] M. L. Boucher, D. R. Peacor, *Z. Kristallogr.* **1968**, 126, 98–111.
- [4] B. A. Maksimov, V. P. Kalinin, B. V. Merinov, V. V. Ilyukhin, N. V. Belov, *Dokl. Akad. Nauk SSSR* **1980**, 252, 875–879.
- [5] Terms like “*neuner*” chain were coined by Liebau (ref. [1]) and are derived from the German words *neun* etc., which means nine etc. Similar terms exist for chains with other periodicities such as *achter* (8), *zehner* (10), *zwölfer* (12), *vierzehner* (14), *einundzwanziger* (21) and *vierundzwanziger* (24). This means that the repeating unit in a chain contains 8, 9, 10 etc. tetrahedra.

- [6] C. Martin, I. Tordjman, A. Durif, *Z. Kristallogr.* **1975**, 141, 403–411.
- [7] E. Cannillo, F. Mazzi, J. H. Fang, P. D. Robinson, Y. Ohya, *Am. Mineral.* **1971**, 56, 427–446.
- [8] E. P. Meagher, *Am. Mineral.* **1976**, 61, 67–73.
- [9] V. V. Bakakin, N. V. Belov, S. V. Borisov, L. P. Solovyeva, *Am. Mineral.* **1970**, 55, 1167–1181.
- [10] M. H. Zöller, E. Tillmanns, G. Hentschel, *Z. Kristallogr.* **1992**, 200, 115–126.
- [11] A. A. Voronkov, Y. A. Pyatenko, *Sov. Phys. Crystallogr.* **1967**, 12, 258–265.
- [12] A. Rulmont, P. Tarte, *J. Solid State Chem.* **1988**, 75, 244–250.
- [13] R. Kniep, G. Gözel, B. Eisenmann, C. Röhr, M. Asbrand, M. Kizilyalli, *Angew. Chem. Int. Ed. Engl.* **1994**, 33, 749–751; *Angew. Chem.* **1994**, 106, 791–793.
- [14] S. D. Kloß, W. Schnick, *Inorg. Chem.* **2018**, 57, 4189–4195.
- [15] A. Marchuk, L. Neudert, O. Oeckler, W. Schnick, *Eur. J. Inorg. Chem.* **2014**, 3427–3434.
- [16] S. D. Kloß, A. Weis, S. Wandelt, W. Schnick, *Inorg. Chem.* **2018**, 57, 4164–4170.
- [17] H. Kageyama, K. Hayashi, K. Maeda, J. P. Attfield, Z. Hiroi, J. M. Rondinelli, K. R. Poeppelmeier, *Nat. Commun.* **2018**, 9, 772–787.
- [18] K. Senevirathne, C. S. Day, M. D. Gross, A. Lachgar, N. A. W. Holzwarth, *Solid State Ionics* **2013**, 233, 95–101.
- [19] E. Mugnaioli, S. J. Sedlmaier, O. Oeckler, U. Kolb, W. Schnick, *Eur. J. Inorg. Chem.* **2012**, 121–125.
- [20] S. D. Kloß, W. Schnick, *Angew. Chem. Int. Ed.* **2019**, 58, 7933–7944; *Angew. Chem.* **2019**, 131, 8015–8027.
- [21] S. D. Kloß, L. Neudert, M. Döblinger, M. Nentwig, O. Oeckler, W. Schnick, *J. Am. Chem. Soc.* **2017**, 139, 12724–12735.
- [22] W. Schnick, J. Lücke, *Z. Anorg. Allg. Chem.* **1990**, 588, 19–25.
- [23] S. J. Sedlmaier, S. R. Römer, W. Schnick, *Z. Anorg. Allg. Chem.* **2011**, 637, 2228–2232.
- [24] F. Fahrnbauer, T. Rosenthal, T. Schmutzler, G. Wagner, G. B. M. Vaughan, J. P. Wright, O. Oeckler, *Angew. Chem. Int. Ed.* **2015**, 54, 10020–10023; *Angew. Chem.* **2015**, 127, 10158–10161.
- [25] S. D. Kloß, N. Weidmann, R. Niklaus, W. Schnick, *Inorg. Chem.* **2016**, 55, 9400–9409.
- [26] Y. Ni, J. M. Hughes, A. N. Mariano, *Am. Mineral.* **1995**, 80, 21–26.
- [27] A. Stock, H. Grüneberg, *Ber. Dtsch. Chem. Ges.* **1907**, 40, 2573–2578.
- [28] H. Huppertz, *Z. Kristallogr.* **2004**, 219, 330–338.
- [29] A. A. Coelho, *TOPAS v. 5.0*, Coelho Software, Brisbane, Australia, **2012**.
- [30] Gatan Inc., *Digital Micrograph*, Pleasanton, California, USA, **1999**.
- [31] J. L. Lábár, *Ultramicroscopy* **2005**, 103, 237–249.
- [32] P. A. Stadelmann, *JEMS*; CIME-EPFL, Saas-Fee, Switzerland, **2008**.
- [33] P. A. Stadelmann, *Ultramicroscopy* **1987**, 21, 131–146.
- [34] Emispec Systems Inc., *ES Vision*, Tempe, Arizona, USA, **2002**.
- [35] J.-C. Labiche, O. Mathon, S. Pascarelli, M. A. Newton, G. G. Ferre, C. Curfs, G. Vaughan, A. Homs, D. F. Carreiras, *Rev. Sci. Instrum.* **2007**, 78, 091301.
- [36] Agilent Technologies, *CrysAlis Pro*, Yarnton, Oxfordshire, England, **2015**.
- [37] Bruker AXS, Inc., *XPREP*, Karlsruhe, Germany, **2001**.
- [38] G. Wu, B. L. Rodrigues, P. Coppens, *J. Appl. Crystallogr.* **2002**, 35, 356–359.
- [39] G. M. Sheldrick, *Acta Crystallogr. Sect. C* **2015**, 71, 3–84.
- [40] V. Petříček, M. Dušek, L. Palatinus, *Z. Kristallogr.* **2014**, 229, 345–352.
- [41] K. Brandenburg, *Diamond*; Crystal Impact GbR, Bonn, Germany, **2014**.

Manuscript received: June 23, 2019

Accepted manuscript online: September 2, 2019

Version of record online: October 15, 2019